

# Validation of acetonitrile (CH<sub>3</sub>CN) measurements in the stratosphere and lower mesosphere from the SMILES instrument on the International Space Station

Tamaki Fujinawa<sup>1,2</sup>, Tomohiro O. Sato<sup>1</sup>, Takayoshi Yamada<sup>1</sup>, Seidai Nara<sup>1,3</sup>, Yuki Uchiyama<sup>1,4</sup>, Kodai Takahashi<sup>1,4</sup>, Naohiro Yoshida<sup>5</sup>, and Yasuko Kasai<sup>1,3</sup>

<sup>1</sup>National Institute of Information and Communications Technology, 4-2-1 Nukui-kitamachi, Koganei, Tokyo 184-8795, Japan

<sup>2</sup>National Institute for Environmental Studies, 16-2 Onogawa, Tsukuba, Ibaraki 305-0053, Japan

<sup>3</sup>University of Tsukuba, 1-1-1 Tennoudai, Tsukuba, Ibaraki 305-8577, Japan

<sup>4</sup>Tokyo Gakugei University, 4-1-1 Nukui-kitamachi, Koganei, Tokyo 184-8501, Japan

<sup>5</sup>Earth-Life Science Institute, Tokyo Institute of Technology, IE-1, 2-12-1, Oookayama, Meguro-ku, Tokyo 152-8550, Japan

**Correspondence:** Y. Kasai (ykasai@nict.go.jp)

**Abstract.** Acetonitrile (CH<sub>3</sub>CN) is a volatile organic compound (VOC) and a potential tracer of biomass burning. We evaluated the capability of using observations derived from the Superconducting Submillimeter-Wave Limb-Emission Sounder (SMILES) on the International Space Station (ISS) to measure CH<sub>3</sub>CN profiles. The error in a CH<sub>3</sub>CN vertical profile from the Level-2 research (L2r) product version 3.0.0 was estimated by theoretical error analysis and also compared with other instrumental measurements. We estimated the systematic and random errors to be ~ 5.8 ppt (7.8 %) and 25 ppt (60 %), respectively, for a single observation at 15.7 hPa in the Tropics, where the CH<sub>3</sub>CN measurements are enhanced. The major source of systematic error was the pressure broadening coefficient, and its contribution to the total systematic error was approximately 60 % in the middle stratosphere (15.7–4.8 hPa). The random error decreased to less than 40 % after averaging 10 profiles in the pressure range of 28.8–1.6 hPa. The total error due to uncertainties in other molecular spectroscopic parameters was comparable (2.8 ppt) to that of CH<sub>3</sub>CN spectroscopic parameters. We compared the SMILES CH<sub>3</sub>CN profiles with those of the Microwave Limb Sounder (MLS) on the Aura satellite (version 4.2). The SMILES CH<sub>3</sub>CN values were consistent with those from MLS within the standard deviation (1  $\sigma$ ) of the MLS observations. The difference between the SMILES and MLS CH<sub>3</sub>CN profiles increased with altitude and was within 20–35 ppt (20–260 %) at 15.7–1.6 hPa. We observed discrepancies of 5–10 ppt (10–30 %) between the SMILES CH<sub>3</sub>CN profiles observed by different spectrometers, and hence, we do not recommend merging SMILES CH<sub>3</sub>CN profiles derived from different spectrometers. We found that SMILES CH<sub>3</sub>CN VMR in the upper stratosphere has a seasonal maximum in February.

## 1 Introduction

Air pollution caused by biomass burning (BB) has become a serious problem with population growth (Marlon et al., 2008). BB events are important sources of various trace gases and particles in the atmosphere (Eagan et al., 1974; Crutzen et al., 1979). The study of atmospheric gas species associated with BB is significant because early estimates of pyrogenic emissions

suggested that some atmospheric pollutants from BB could be comparable to those from fossil fuel burning (Crutzen and Andreae, 1990; Seiler and Crutzen, 1980). These emissions could, therefore, significantly affect the global atmosphere and its temperatures (Andreae, 1983).

Acetonitrile ( $\text{CH}_3\text{CN}$ ) is a good tracer for BB as 90–95 % of  $\text{CH}_3\text{CN}$  comes from wildfires (Li et al., 2003). The mean  
25 lifetime of  $\text{CH}_3\text{CN}$  in the atmosphere is about 6.6 months, with ocean uptake and reaction with hydroxyl (OH) radicals (Singh et al., 2003; de Gouw, 2003). Chemical loss of  $\text{CH}_3\text{CN}$  due to OH radicals occurs primarily in the stratosphere, whereas oceanic loss is dominant in the troposphere. Carbon monoxide (CO) is also a well-known BB tracer, but it has an atmospheric lifetime of only about 2 months in the free troposphere. CO is also emitted from some anthropogenic sources. Thus,  $\text{CH}_3\text{CN}$  is not only existent for a longer period of time, but is also more specific to BB, and is, therefore, a better tracer. Arnold et al. (1978)  
30 first measured the presence of stratospheric  $\text{CH}_3\text{CN}$  from the composition of positive ions using active chemical ionization mass spectrometry.  $\text{CH}_3\text{CN}$  has also been detected using balloon-borne and airborne measurements in the lower stratosphere (Knop and Arnold, 1987; Schneider et al., 1997). More recently, satellite observations of  $\text{CH}_3\text{CN}$  in the lower stratosphere have been measured using several satellite instruments, such as the Microwave Limb Sounder (MLS) onboard the UARS (Upper Atmosphere Research Satellite) (Barath et al., 1993), the Atmospheric Chemistry Experiment Fourier Transform Spectrometer  
35 (ACE-FTS) onboard the Scisat-1 (Bernath, 2001), the MLS onboard the Aura (Waters et al., 2006), and the Superconducting Submillimeter-Wave Limb-Emission Sounder (SMILES) onboard the JEM (Japanese Experiment Module) of the International Space Station (ISS) (Kikuchi et al., 2010). Previous research reported the volume mixing ratio (VMR) of  $\text{CH}_3\text{CN}$  mainly in the upper troposphere and lower stratosphere (UTLS) (Livesey et al., 2001, 2004; Harrison and Bernath, 2013). However, there are only a few reports of the  $\text{CH}_3\text{CN}$  VMR in the lower stratosphere to mesosphere.

40 Here, we derived vertical distribution profiles of  $\text{CH}_3\text{CN}$  between the lower stratosphere and mesosphere from SMILES observations. We also performed a validation analysis comparing these results with the Aura/MLS observation data.

## 2 SMILES $\text{CH}_3\text{CN}$ observations

The JEM/SMILES was operated from October 12, 2009 until April 21, 2010 on the ISS (Kikuchi et al., 2010). The ISS has a non sun-synchronous orbit and an inclination angle of  $51.6^\circ$  to the equator, which enables it to observe the atmosphere at  
45 various local solar times. The antenna field of view of the SMILES instrument was set to point in a  $45^\circ$  direction leftward from the ISS orbital motion. Low temperature system noise ( $T_{sys} \sim 350$  K) was achieved using four kelvin cooled submillimeter wave superconductive heterodyne receivers (Ochiai et al., 2011). This noise level is ten times lower than that in the previous observations (Kikuchi et al., 2010). A summary of characteristics for SMILES observation is shown in Tab. 1.

The targeted  $\text{CH}_3\text{CN}$  transition at 624.82 GHz for  $(J, K) = (33, 3) - (33, 4)$  is allocated with a frequency region of Band-A  
50 (624.32–625.52 GHz) as shown in Fig. 1. SMILES employed two Acousto Optical Spectrometers (AOSs) with a bandwidth of 1.2 GHz, denoted as AOS1 and AOS2. The band configuration for AOS1 and AOS2 are summarized in Tab. 2. The date of observations made by AOS1 and AOS2 are shown in Fig. 2. The two AOSs detect Band-A, B, or C separately, enabling SMILES to observe two of the three bands simultaneously.

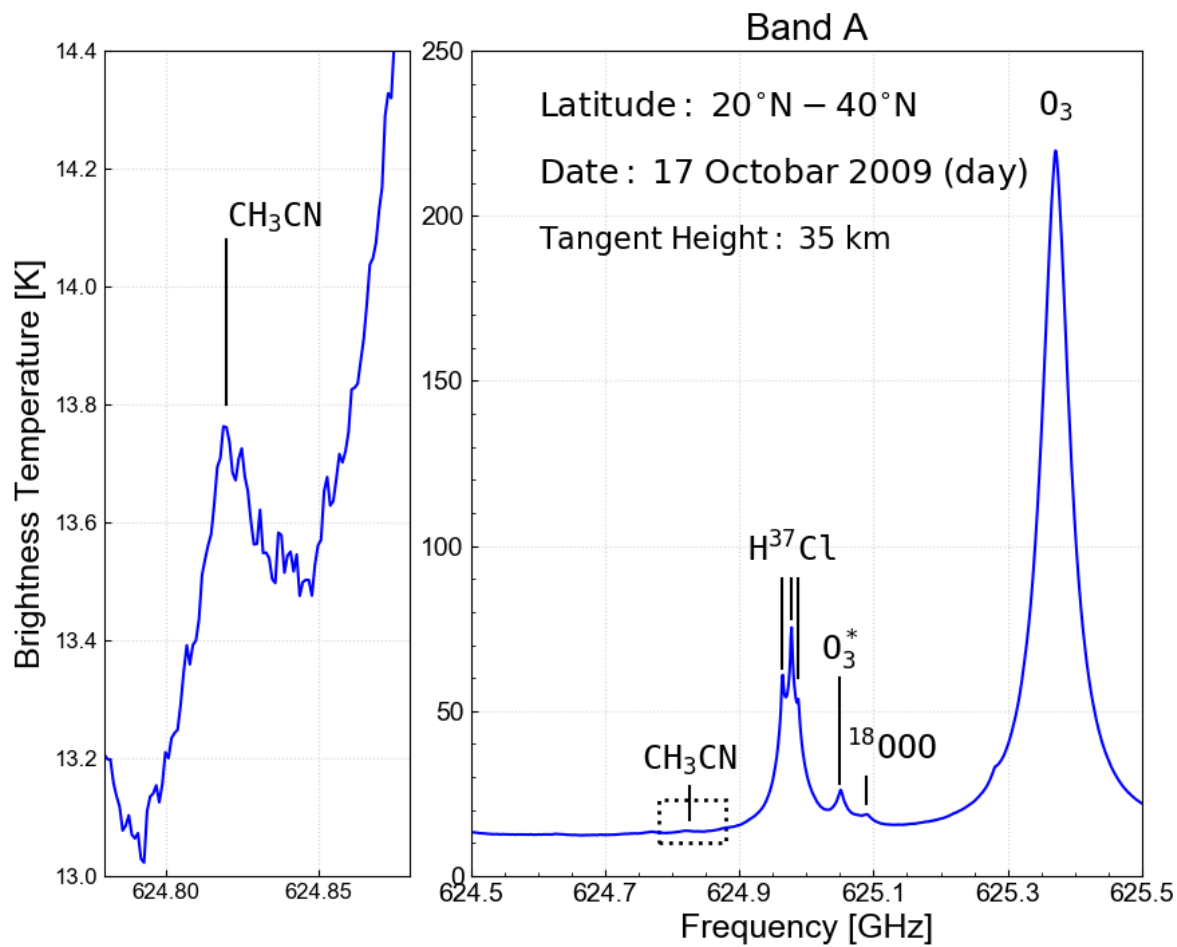


**Figure 1.** Example of a SMILES spectrum (L1b ver. 008) of Band-A. 50 scans were accumulated in a tangent height of  $35 \pm 2.5$  km over the daytime on October 17, 2009.

**Table 1.** SMILES characteristics.

Parameter	Characteristics
Orbit	Non sun-synchronous orbit ~ 91 min orbital period
Latitude coverage	38° S–65° N (nominal)
Integration time	0.47 sec
Number of data	1630 scan per day
Frequency range	624.32–625.52 GHz (Band-A) 625.12–626.32 GHz (Band-B) 649.12–650.32 GHz (Band-C)
Receiver system and SIS mixers and HEMT amplifiers <sup>†</sup> Spectrometers	Acousto Optical Spectrometers (AOS1 and AOS2)
Frequency resolution	0.8 MHz
System noise temperature	~ 350 K

<sup>†</sup> SIS: Superconductor–insulator–superconductor mixer;

HEMT: High electron mobility transistor

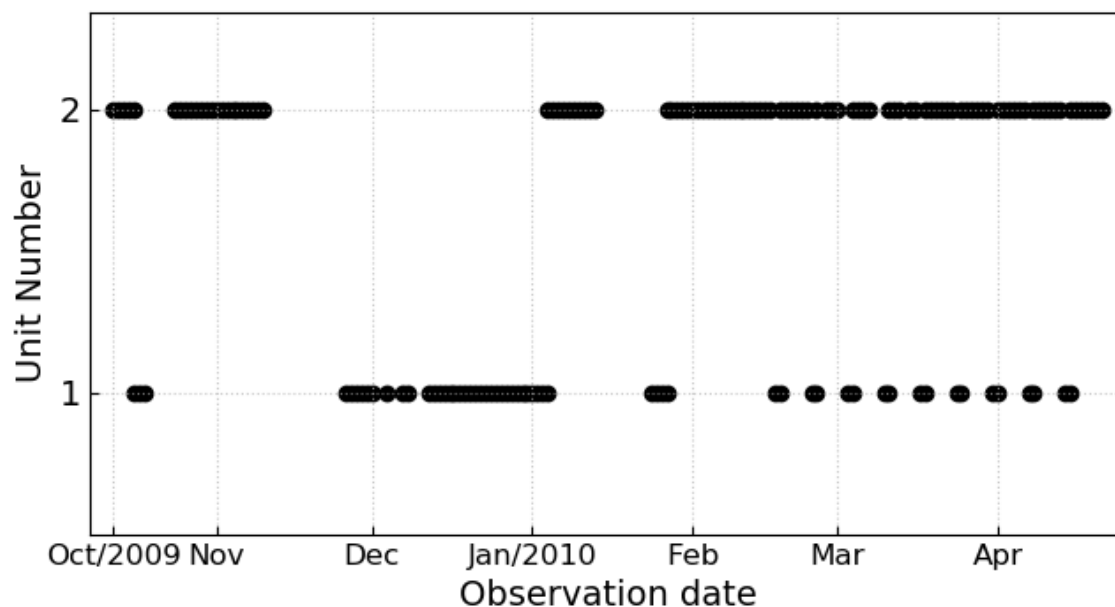


**Figure 2.** The distribution of AOS unit number for the SMILES CH<sub>3</sub>CN observation data.

**Table 2.** Band configurations

Band config. no.	AOS1	AOS2
#1	Band-A	Band-B
#2	Band-C	Band-B
#3	Band-C	Band-A

SMILES Level 2 research (L2r) product version 3.0.0 (v3.0.0) was used in this study. The CH<sub>3</sub>CN VMR profile was retrieved from the measurement spectra data of the Level-1b (L1b) version 008. Major improvements of the v3.0.0 over the previous version 2.1.5 included the AOS response function and the a priori temperature profile. This version of L2r product was derived from the Level-1b (L1b) version 008 calibrated spectra, which used version 5.2 of the Goddard Earth Observing System Model (GEOS-5.2) as a priori information (e.g., O<sub>3</sub> VMR profile, temperature and pressure profiles) (Rienecker et al., 2008). The details can be found in the JEM/SMILES L2r data product guideline (see <http://smiles.nict.go.jp/pub/data/index.html>). The optimal estimation method (OEM) was used for the retrieval processing. The OEM leads to the maximum a posteriori probability solution (Rodgers, 2000), which minimizes the value of  $\chi^2$  described below.

$$\chi^2 = [\mathbf{y} - \mathbf{F}(\mathbf{x}, \mathbf{b})]^T \mathbf{S}_y^{-1} [\mathbf{y} - \mathbf{F}(\mathbf{x}, \mathbf{b})] + [\mathbf{x}_a - \mathbf{x}]^T \mathbf{S}_a^{-1} [\mathbf{x}_a - \mathbf{x}] \quad (1)$$

where  $\mathbf{F}(\mathbf{x}, \mathbf{b})$  is the forward model depending on  $\mathbf{x}$  state vector and on the known model parameters  $\mathbf{b}$ ,  $\mathbf{S}_y^{-1}$  the measurement covariance matrix,  $\mathbf{x}_a$  the a priori state of  $\mathbf{x}$ , and  $\mathbf{S}_a$  the a priori covariance matrix. Detailed retrieval algorithm of L2r product can be found in Baron et al. (2011) and Sato et al. (2012).

Quality of the retrieval processing was quantified by the chi-squared statics, or goodness of the fit (Eq. 1), and the measurement response ( $\mathbf{m}$ ) was defined as,

$$\mathbf{m}[i] = \sum_j |\mathbf{A}[i, j]| \quad (2)$$

$$\mathbf{A} = \frac{\partial \hat{\mathbf{x}}}{\partial \mathbf{y}} = \mathbf{D}\mathbf{K} \quad (3)$$

$$\mathbf{D} = \frac{\partial \hat{\mathbf{x}}}{\partial \mathbf{y}} = (\mathbf{K}^T \mathbf{S}_y^{-1} \mathbf{K} + \mathbf{S}_a^{-1})^{-1} \mathbf{K}^T \mathbf{S}_y^{-1} \quad (4)$$

$$\mathbf{K} = \frac{\partial \mathbf{y}}{\partial \mathbf{x}} \quad (5)$$

where  $\hat{\mathbf{x}}$  is the solution of the retrieval,  $\mathbf{A}$  the averaging kernel,  $\mathbf{D}$  the contribution function, and  $\mathbf{K}$  the weighting function.  $\mathbf{m}$ ,  $\mathbf{A}$  and  $\mathbf{D}$  were derived using  $\mathbf{K}$  (Urban et al., 2004). Details on  $\mathbf{m}$  are explained by Sato et al. (2014). The  $\chi^2$  of CH<sub>3</sub>CN for v3.0.0

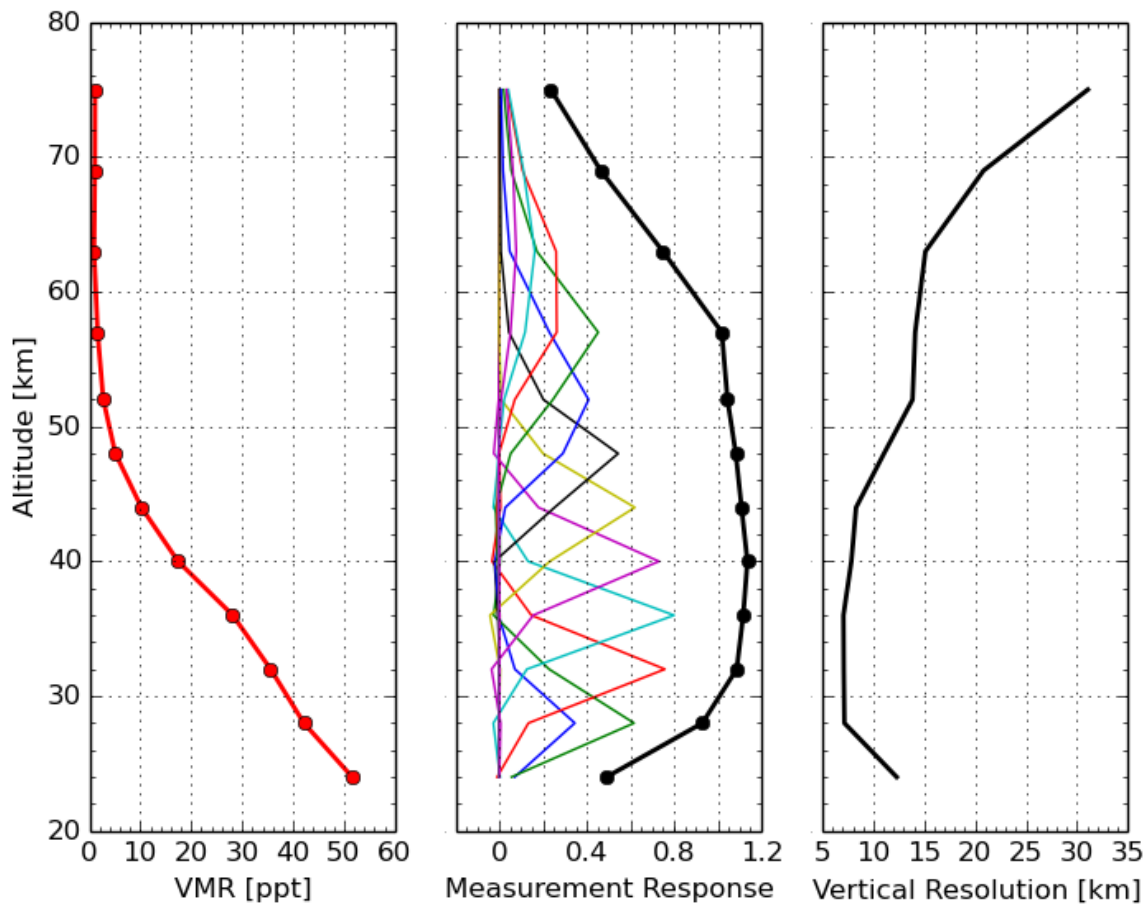


**Figure 3.** (*Left*) Vertical profile of CH<sub>3</sub>CN retrieved from a single spectral scan on November 4th 2009, in the Tropics at a latitude less than 20°. (*Middle*) The averaging kernel by altitude, for each measurement (color line), and the measurement response (solid black line). (*Right*) The vertical resolution of the profile, defined as the full width at half maximum (FWHM).

had a range of 0.4–0.6. In cases where the measurement response was low, the information was retrieved from the a priori state. Here, the data selection thresholds of  $\chi^2$  and measurement response were set as  $\chi^2 < 0.6$  and  $\mathbf{m} > 0.80$ , respectively.

Figure 3 shows an example of the retrieval results from a single spectral scan on November 4, 2009, in the Tropics at a latitude less than  $20^\circ$ , including the retrieved  $\text{CH}_3\text{CN}$  vertical profile, averaging kernel, and vertical resolution. The vertical resolution was defined as the full width at half maximum (FWHM) for each row of the averaging kernel matrix. The measurement response of retrieved  $\text{CH}_3\text{CN}$ , shown as a black solid line in the middle panel of Fig. 3, is the sum of elements from the averaging kernel at each altitude grid. The measurement response was almost one from 30 to 55 km, with a vertical resolution of 7–15 km, decreasing with altitude.

### 85 3 Theoretical error analysis

We theoretically estimated the error in deriving  $\text{CH}_3\text{CN}$  profiles from SMILES observations by perturbing the model parameters in a forward model (Sato et al., 2012; Kasai et al., 2013; Sagawa et al., 2013). We used a typical  $\text{CH}_3\text{CN}$  profile derived using observations from the Tropics, where BB (a major source of  $\text{CH}_3\text{CN}$ ) frequently occurs. The total error ( $\mathbf{E}_{total}$ ) is given by

$$90 \quad \mathbf{E}_{total}[i] = \sqrt{\mathbf{E}_n^2[i] + \mathbf{E}_s^2[i] + \mathbf{E}_p^2[i]}, \quad (6)$$

where  $\mathbf{E}_n$  is the error due to spectral noise,  $\mathbf{E}_s$  the smoothing error, and  $\mathbf{E}_p$  the model parameter error. The error due to the spectral calibration was ignored in this study, because the L1b data was updated in this version, and the error due to the spectral calibration was not significant according to previous SMILES error analyses (e.g. Sato et al., 2012).

Error  $\mathbf{E}_n$  and  $\mathbf{E}_s$  were calculated by the following equation

$$95 \quad \mathbf{E}_n[i] = \sqrt{\mathbf{S}_n[i, i]}, \quad (7)$$

where

$$\mathbf{S}_n = \mathbf{D}\mathbf{S}_y\mathbf{D}^T, \quad (8)$$

and

$$\mathbf{E}_s[i] = \sqrt{\mathbf{S}_s[i, i]}, \quad (9)$$

100 where

$$\mathbf{S}_s = (\mathbf{A} - \mathbf{U})\mathbf{S}_a(\mathbf{A} - \mathbf{U})^T. \quad (10)$$

Here,  $\mathbf{S}_n$  and  $\mathbf{S}_s$  are the error covariance matrices for measurement noise and the errors from  $\mathbf{S}_a$ , respectively.  $\mathbf{U}$  is the unit matrix.

The model parameter error  $\mathbf{E}_p$  includes errors caused by uncertainties in the parameters used in both the forward and inversion calculations. Error sources for the model parameters are summarized in Tab. 3. Error related to each of the individual model parameters was calculated using the perturbation method following Sato et al. (2012). The total error  $\mathbf{E}_p$  for all of the parameters was calculated using the root sum square of the individual errors.

Figure 4 shows the estimated systematic errors. The left panel (a) shows the uncertainties in the AOS response function ("AOS"), the antenna beam pattern ("Antenna"), the spectral line strength ("Strength"), the air pressure broadening coefficient (" $\gamma$ "), its temperature dependence (" $n$ "), and their root-sum-square ("Total"). The largest error source  $\sim 2$  ppt (5 %) was from the air pressure broadening coefficient (" $\gamma$ ") across the entire pressure range, followed by those from the line intensity ("Strength") and temperature dependence of air pressure broadening coefficient (" $n$ ") ( $\simeq 1.5$  ppt). The error from spectroscopic parameters was more significant than that from the instrumental functions.

**Table 3.** Potential error sources.

Error source	Uncertainty
Spectroscopic parameter of CH <sub>3</sub> CN	
Line intensity (Strength)	1 %
Air pressure broadening ( $\gamma$ )	3 %
Temperature dependence of $\gamma$ ( $n$ )	10 %
Instrumental functions	
AOS response function (AOS)	10 %
Antenna scan (Antenna)	2 %
Impact from other species	
H <sup>37</sup> Cl air pressure broadening (H <sup>37</sup> Cl $\gamma$ )	3 %
Temperature dependence of H <sup>37</sup> Cl $\gamma$ (H <sup>37</sup> Cl $n$ )	10 %
O <sub>3</sub> air pressure broadening (O <sub>3</sub> $\gamma$ )	3 %
O <sub>3</sub> temperature dependence of O <sub>3</sub> $\gamma$ (O <sub>3</sub> $n$ )	10 %

In Band-A, O<sub>3</sub> and H<sup>37</sup>Cl are observed near the CH<sub>3</sub>CN transition (See Fig. 1). The spectral shapes of O<sub>3</sub> and H<sup>37</sup>Cl should, therefore, influence the retrieval of the CH<sub>3</sub>CN VMR profiles. To estimate the influence from the other spectral lines, the error due to the spectroscopic parameters  $\gamma$  and its temperature dependence  $n$  of the O<sub>3</sub> and H<sup>37</sup>Cl lines were also calculated.  $\gamma$  and temperature dependence of  $\gamma$  were perturbed for each species, and are expressed as "O<sub>3</sub> $\gamma$ ", "O<sub>3</sub> $n$ ", "H<sup>37</sup>Cl $\gamma$ " and "H<sup>37</sup>Cl $n$ ". As shown in Fig. 4 (b), "H<sup>37</sup>Cl $\gamma$ " is the largest error source, the maximum absolute difference of which was 1.1 ppt. Error analyses performed for O<sub>3</sub> and ClO demonstrated that the error caused by other molecular spectral lines was negligible as they have high, isolated line strengths (Sato et al., 2012; Sagawa et al., 2013; Kasai et al., 2013). In the case of CH<sub>3</sub>CN retrieval, however, the total error caused by uncertainties in other molecular spectroscopic parameters was comparable to the error caused by CH<sub>3</sub>CN spectroscopic parameters. The error due to H<sup>37</sup>Cl was larger than that from O<sub>3</sub> at each pressure level.



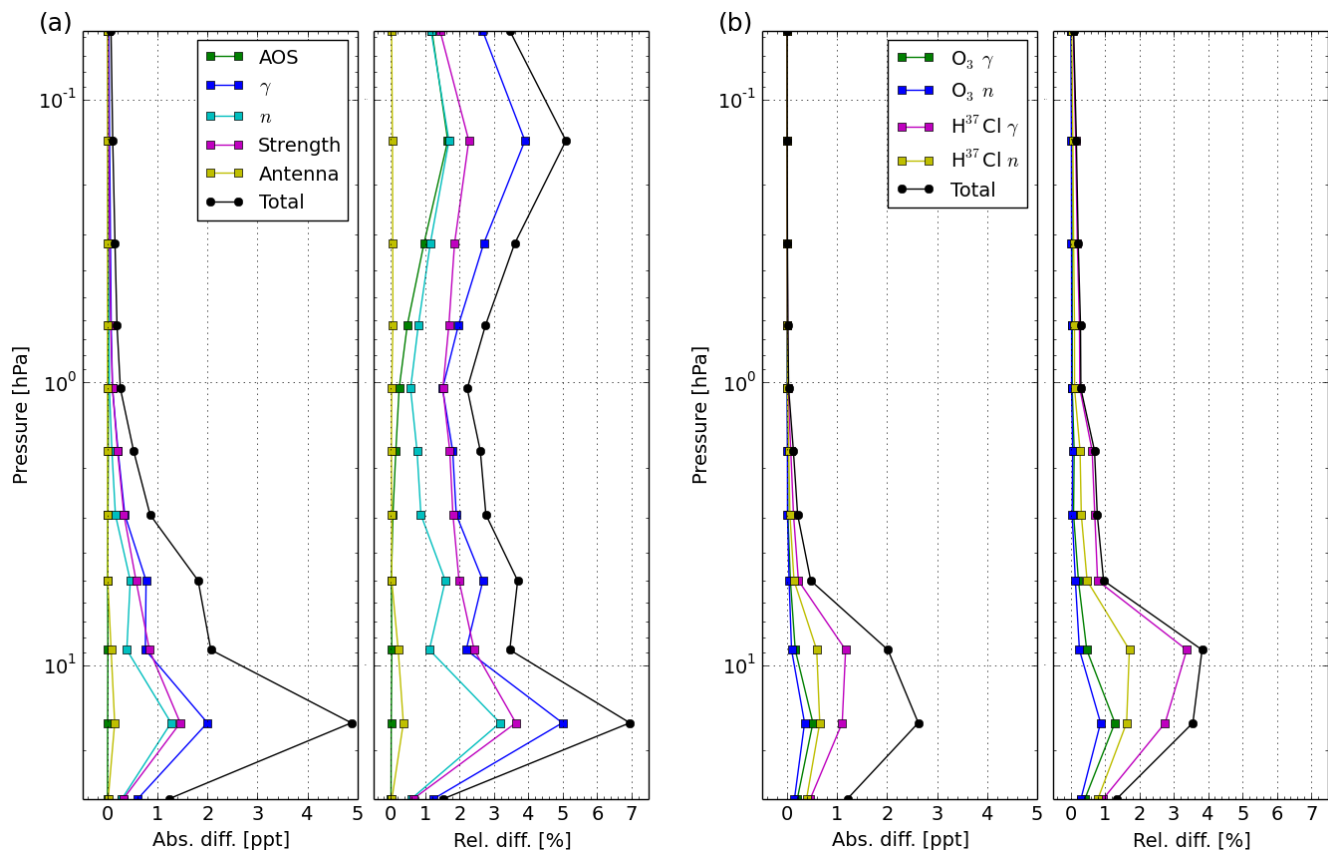


**Figure 4.** (a) Summary of absolute and relative differences derived from systematic errors of  $CH_3CN$  retrieval caused by uncertainties in the spectral parameters and (b) instrumental functions derived from single scan spectrum observed on November 4, 2009, in the Tropics, as shown in Fig. 3. The black line indicates the total error calculated by root-sum-square of all assumed error sources.

The measurement noise and smoothing error from a single scan are shown in Fig. 5 (a). These errors were considered as a random error for a  $CH_3CN$  profile. SMILES  $CH_3CN$  total error consists of both the systematic and random errors. Figure 5  
 125 (b) shows the total systematic error, the random error, and the total error averaged by the number of profiles ( $N = 1, 10$  and 100). For a single scan, the random error was larger than the systematic error. However, the random error averaged by 100 profiles was comparable to the systematic error, except for the highest systematic error found at a pressure level of about 1 hPa.

#### 4 Comparison with Aura/MLS

In this section, we compare SMILES  $CH_3CN$  observations with Aura/MLS observations and discuss the validity of SMILES  
 130 observations.

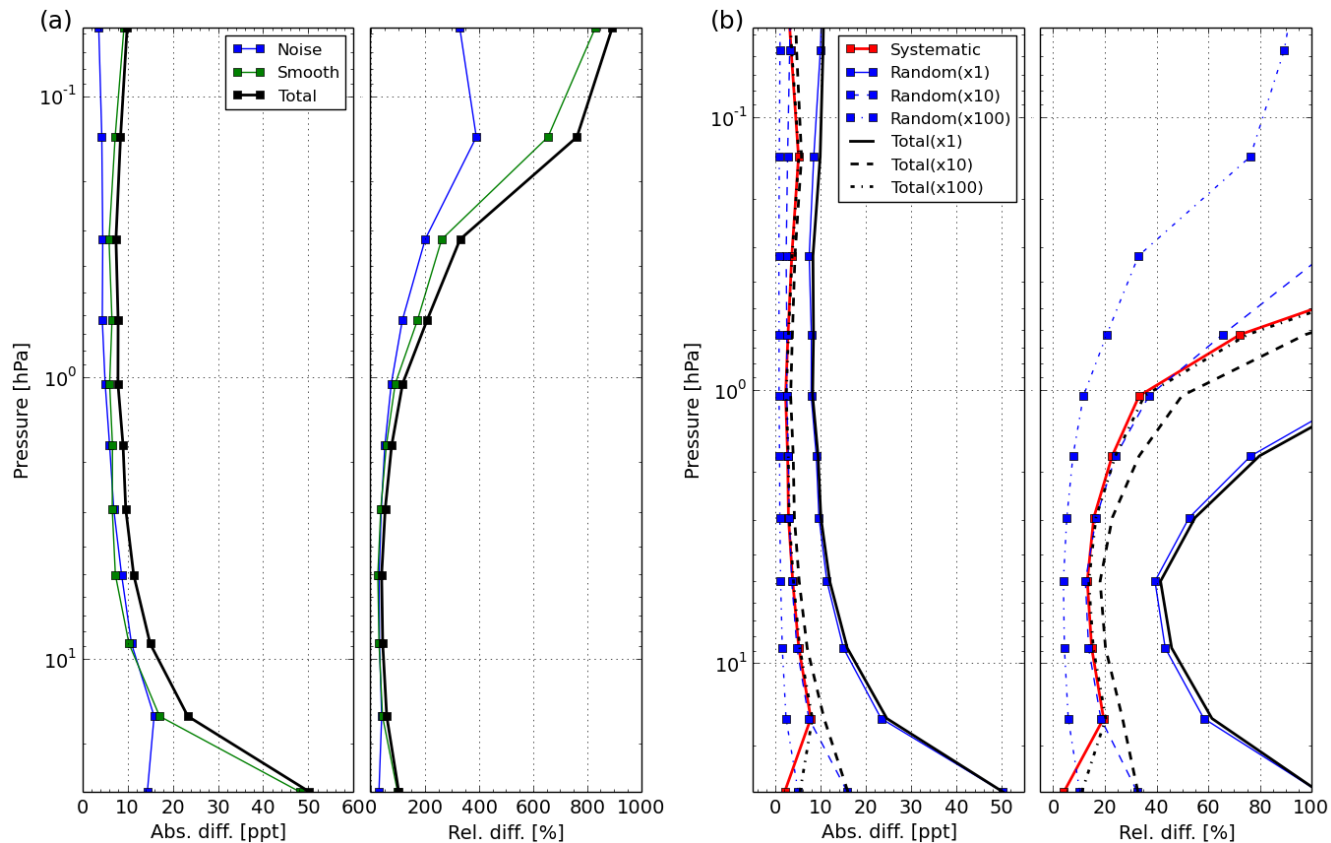


**Figure 5.** (a) Summary of absolute and relative differences derived from random errors of  $\text{CH}_3\text{CN}$  retrieved from a SMILES single scan observation as shown in Fig. 4. (b) Summary of absolute and relative differences derived from random (blue), systematic (red), and total (black) errors in the SMILES  $\text{CH}_3\text{CN}$  retrieval for the averaging of  $N$  profiles ( $N = 1, 10, 100$ ). The number in the legend is the accumulating profile number.

Figure 6 shows (a) a  $\text{CH}_3\text{CN}$  vertical profiles observed by AOS1 and AOS2, (b and c) and the absolute and relative differences between AOS1 and AOS2 observed in Equatorial regions ( $20^\circ \text{S} - 20^\circ \text{N}$ ) from March until April 2010, when AOS1 and AOS2 were alternating at a ratio of 1:3. The error bars shown in the left panel of Fig. 6 are standard deviations ( $1\sigma$ ) of the  $\text{CH}_3\text{CN}$  VMR observations retrieved at SMILES pressure grids for AOS1 (red) and AOS2 (blue). The relative difference between AOS1 and AOS2 is approximately 12 ppt (30%) with the maximum at 15.7 hPa. It is likely that these discrepancies between the two AOSs result from sensitivity differences. We believe that the sensitivity differences indicate inherent sensitivity differences between the two AOSs derived from instrumental characterization determined during manufacturing. Kasai et al. (2013) also reported the discrepancies between the two different AOSs, albeit for the analysis of ozone profiles using the SMILES L2 version 2.1.5 product. As mentioned above, in this analysis, we used the SMILES L2r version 3.0.0 product that improves the AOS response function. However, there may still be disagreement between the two AOSs. The relative differ-

ence between the two AOSs decreases to less than 10 % at an upper altitude than 4.8 hPa, except at 0.3 hPa, showing a good agreement of the two AOS observations from the middle stratosphere.

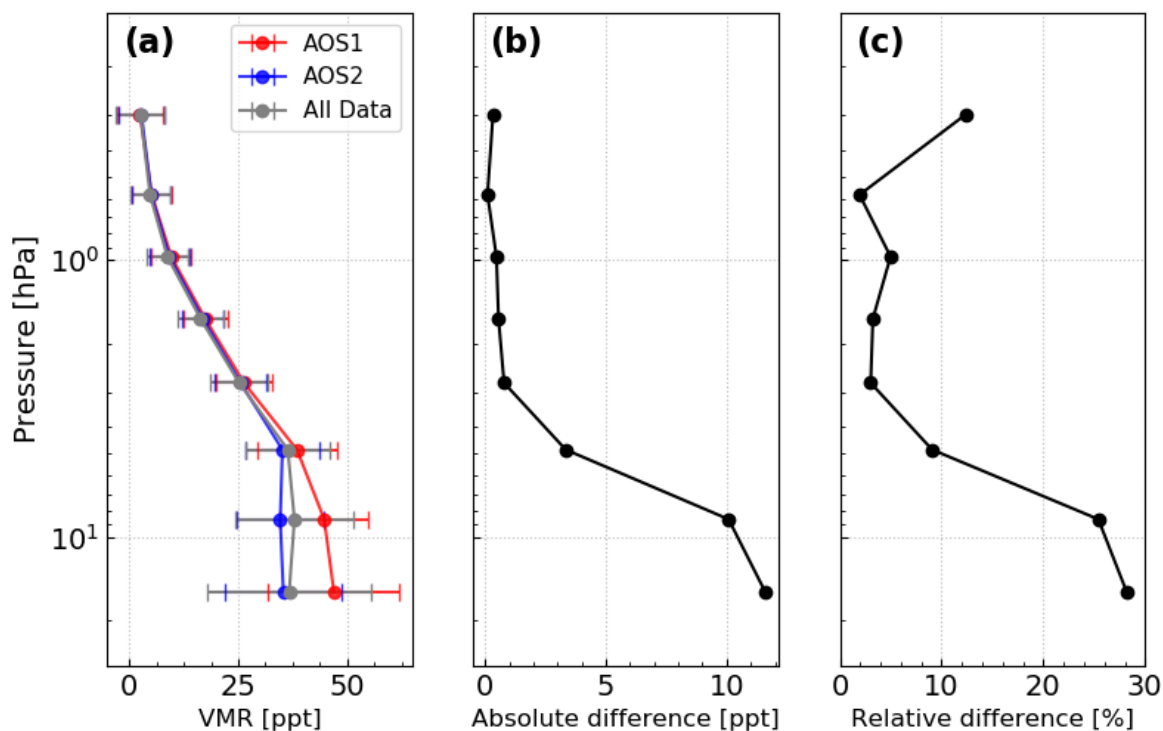


**Figure 6.** (a) Vertical profiles of CH<sub>3</sub>CN from AOS1, AOS2, and the sum of AOS1 and AOS2 in the Equatorial region from 20°S to 20°N, from March until April 2010. Each line indicates the averaged VMR from AOS1 observations (red line), AOS2 observations (blue line), and the sum of AOS1 and AOS2 observations (grey line). (b) The absolute difference between AOS1 and AOS2 ( $AOS1 - AOS2$ ). (c) The relative difference between AOS1 and AOS2 ( $(AOS1 - AOS2)/M$  when  $M$  is  $(AOS1 + AOS2)/2$ ).

We also investigated seasonal variation of SMILES CH<sub>3</sub>CN observations for each altitude grid as shown in Fig. 7. This figure shows daily scatter plots and daily averages for AOS1 (red shaded) and AOS2 (blue shaded) observations. The red circles and bars represent the daily mean values and 1  $\sigma$  standard deviations, when more than one hundred observation points were obtained in one day. As shown in Fig. 2, at lower altitudes (28 km to 36 km), the difference between the two AOSs observations was significantly larger, especially from December until the beginning of January. However, in the upper stratosphere, there was no difference between the two AOS observations, and the standard deviations decreased with altitude. In terms of seasonality, CH<sub>3</sub>CN levels peaked in February, seen from approximately 40 km to 52 km, where the difference between the two AOSs is negligible.

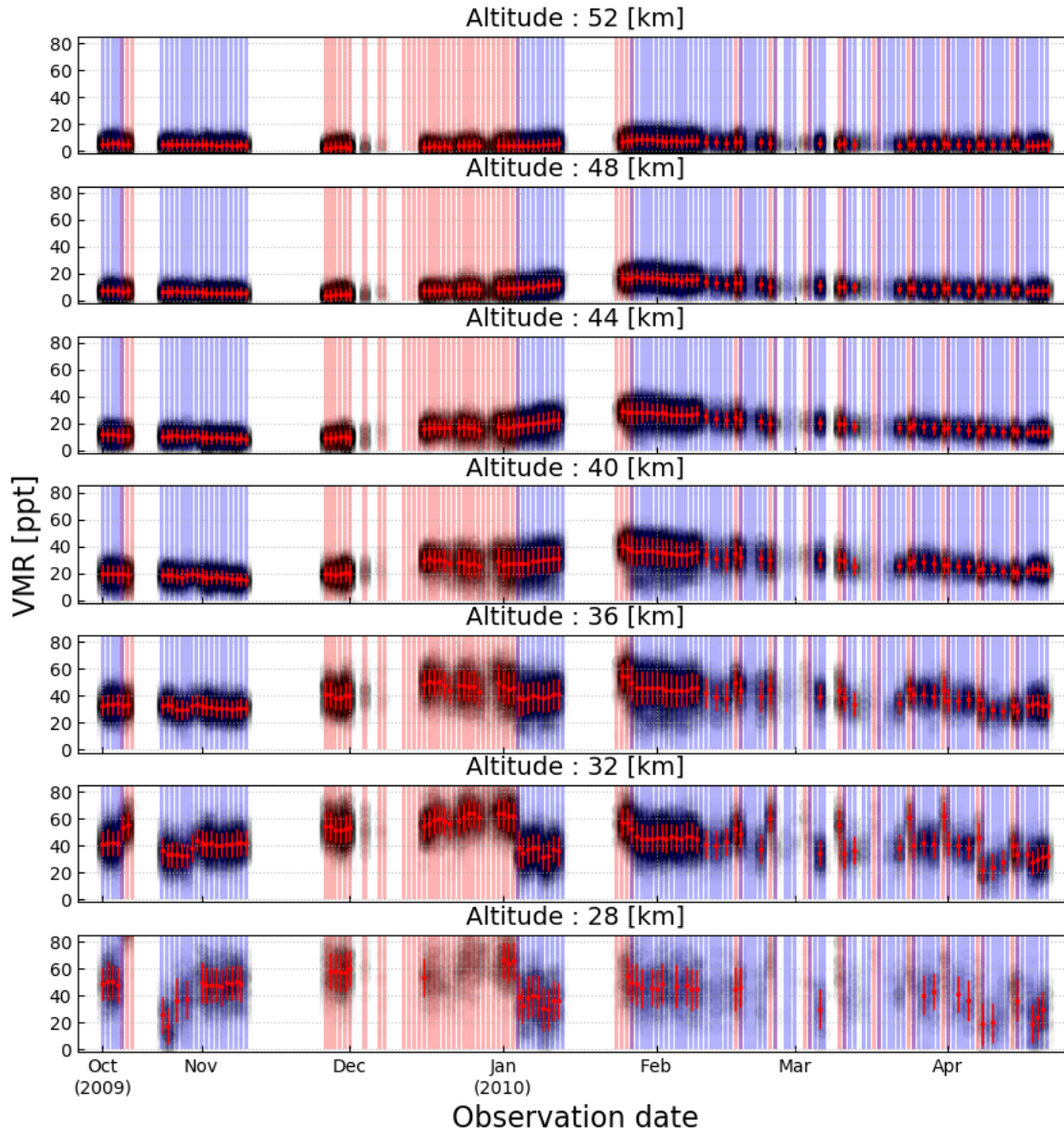


**Figure 7.** Daily scatter and average plots for retrieved  $\text{CH}_3\text{CN}$  observations at each altitude (28–52 km) in the Equatorial region ( $20^\circ\text{S}$ – $20^\circ\text{N}$ ). Solid red lines indicate filtered mean values observed on each day. Error bar indicates  $1\sigma$  standard deviation. Red (blue) shaded areas represent the date observed by AOS1 (AOS2).

**Table 4.** Data quality criteria for SMILES and MLS

Data products	Quality threshold
SMILES v3.0.0	Measurement response > 0.80 Goodness of fit ( $\chi^2$ ) < 0.6 Field-of-view = 0
MLS v4.2	Quality > 1.40 Convergence < 1.05 Status = 0

#### 4.1 Comparison with Aura/MLS v4.2 data

We investigated the difference between CH<sub>3</sub>CN VMRs obtained from SMILES and MLS observations. We set the data quality thresholds and the coincidence selection criteria for the SMILES and MLS observations, as summarized in Tab. 4. The MLS data quality criteria was based on the MLS v4.2 Level-2 data quality and description document.

155 The geolocation and measurement time criteria were determined as follows,

- the distance of measurement location within 300 km;
- difference in the measurement time within 6 h.

We investigated the diurnal variation of SMILES CH<sub>3</sub>CN observations at several altitudes (32 km, 40 km, and 48 km) for AOS1 and AOS2 individual observational periods, and confirmed that there is no diurnal variation for stratospheric CH<sub>3</sub>CN observations.

160 Figure 8 shows the distribution of coincident points satisfying these criteria at 8.6 hPa. The interpolation of VMRs was done using a linear interpolation with respect to the logarithm pressure levels. There are, on average, 10 coincident points in each bin at this pressure level, and the total coincident data number was 17910.

165 For comparing the SMILES and the MLS observations, the mean absolute difference,  $\Delta_{abs}$ , and relative difference,  $\Delta_{rel}$ , at the pressure levels,  $p$ , between coincident CH<sub>3</sub>CN profiles of the two observations were calculated as follows,

$$\Delta_{abs} = \frac{1}{N(p)} \sum_{i=1}^{N(p)} \{x_s(p) - x_m(p)\}, \quad (11)$$

$$\Delta_{rel} = \frac{1}{N(p)} \sum_{i=1}^{N(p)} \frac{\{x_s(p) - x_m(p)\}}{\bar{x}_p}, \quad (12)$$

170 where  $N(p)$  is the number of coincidences at  $p$ ,  $x_s(p)$  and  $x_m(p)$  are the VMRs at  $p$  for SMILES and MLS observations, and the reference ( $\bar{x}_p$ ) is  $\bar{x}_p = \frac{1}{2}(x_s(p) + x_m(p))$ .

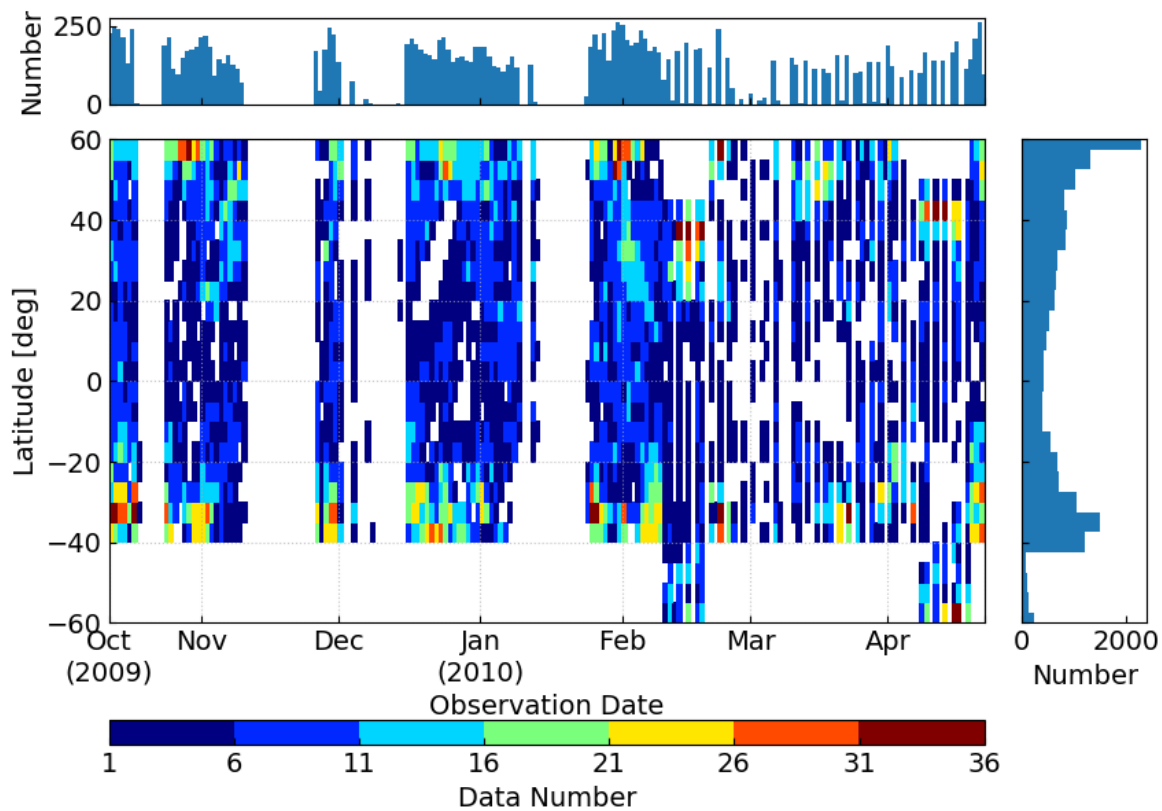


**Figure 8.** Distribution of the data meeting the criteria between October 12, 2009 and April 21, 2010, at 8.6 hPa. Observation date and latitude bins are 1 day and 3°.

#### 4.1.1 Aura/MLS v4.2

The MLS has been onboard the Aura satellite since 2004 and has observed CH<sub>3</sub>CN levels from the lower to upper stratosphere. This satellite was launched in the sun-synchronous orbit with an equator-crossing time 13:45 (ascending) and 01:45 (descending). The daily MLS measurements give 82° S to 82° N latitude coverage. The MLS measures temperature and trace gases (O<sub>3</sub>, CO, H<sub>2</sub>O, HNO<sub>3</sub>, CH<sub>3</sub>CN, etc.) using thermal emission data from the atmosphere. The CH<sub>3</sub>CN VMR values were retrieved from the MLS observation data using the optimal estimation method. Details on the retrieval algorithm is described in Livesey et al. (2006). The MLS uses spectral bands of 118, 190, 240, and 640 GHz, and 2.5 THz, observing CH<sub>3</sub>CN from 640 GHz spectral regions (Waters et al., 2006). MLS Level-2 CH<sub>3</sub>CN profiles were observed in 640 GHz spectral regions. Although

the pressure range of a retrieved MLS CH<sub>3</sub>CN is 147 to 0.001 hPa, the pressure range of CH<sub>3</sub>CN version 4.2.0 is 46–1.0 hPa  
180 (Livesey et al., 2006).

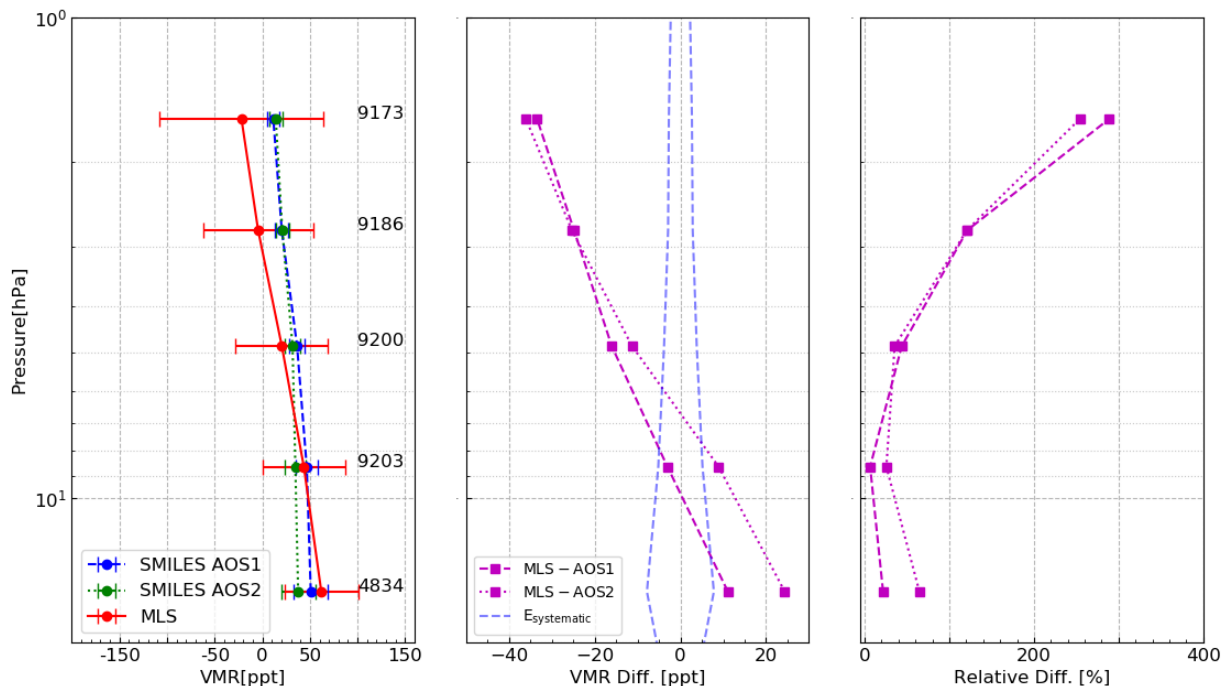
#### 4.1.2 Result of comparisons

Figure 9 shows the vertical profiles, the absolute differences, and the relative differences between SMILES AOS1/AOS2 and  
MLS CH<sub>3</sub>CN observations. The left panel in Fig. 9 indicates good agreement among the three observations in the range from  
15.7 hPa to 4.8 hPa. Across the range of the pressure levels, the absolute difference and the relative difference among the  
185 three observations were -15–25 ppt and 20–80 %, respectively. The difference between the SMILES and the MLS observations  
increases with altitude, from a pressure level of 8.6 hPa. It should be noted that the discrepancies between the two instruments  
were exaggerated at upper pressure levels from 2.8 hPa, although negative values of CH<sub>3</sub>CN VMR derived from MLS have  
no physical meaning. Overall, the variance of SMILES observations is lesser than that of MLS, as SMILES  $T_{sys}$  was more  
than ten times lesser than that of MLS, indicating that SMILES has an advantage in the upper stratosphere. SMILES was also  
190 able to observe CH<sub>3</sub>CN VMR in the upper stratosphere with a much lower uncertainty of ~20 ppt, although the uncertainty  
of MLS CH<sub>3</sub>CN VMR was approximately 100 ppt in the altitude. The differences in the CH<sub>3</sub>CN VMRs observed by the  
two AOSs were sufficiently small in comparison with the difference between SMILES and MLS observations. Theoretical  
systematic error (blue broken lines in the middle panel) derived in Sect. 3 was less than the differences between SMILES and  
MLS observations, except at 8.9 hPa.

195 We also investigated latitudinal and seasonal variations between the two observations. Figure 10 shows the seasonal variation  
of SMILES and MLS CH<sub>3</sub>CN observations, and the absolute differences for each pressure level at coincident points, as a  
function of latitude. The left column represents SMILES CH<sub>3</sub>CN VMR in units of ppt, which were separated into two AOSs  
observations. The middle column represents MLS CH<sub>3</sub>CN VMR, and the right column represents the absolute differences  
between SMILES and MLS observations. At lower altitudes of 15.7 hPa and 8.6 hPa, SMILES observations were overestimated  
200 when compared with the MLS observations, while at upper levels (4.8 hPa~) SMILES observations were underestimated up  
to 40 ppt. At every pressure level, SMILES CH<sub>3</sub>CN VMRs were higher in the Tropics (20° S ~ 20° N). However, in the case  
of MLS observations at higher pressure levels, MLS observations were negatively biased and the trend was not conspicuous.  
The MLS CH<sub>3</sub>CN levels in the Tropics were ambiguous at pressure levels above from 4.8 hPa, indicating that in the upper  
stratosphere, it is hard to observe latitudinal and seasonal trends of CH<sub>3</sub>CN, due to the large uncertainty in MLS observations.  
205 At pressure levels above 4.8 hPa, SMILES CH<sub>3</sub>CN observations in February were greater than those in the other periods,  
which also can be seen in the MLS results. This result indicates that CH<sub>3</sub>CN in the upper stratosphere reaches its seasonal  
maximum in February.

## 5 Conclusions

Our analysis demonstrates the validity of using SMILES observations to measure CH<sub>3</sub>CN profiles. We were able to success-  
210 fully derive vertical profiles and observe seasonal variation of CH<sub>3</sub>CN in the stratosphere, using SMILES observations. This



**Figure 9.** (Left) Mean CH<sub>3</sub>CN VMR values and the standard deviations for SMILES and MLS measurements. The blue and green lines represent the SMILES VMR observed by AOS1 and AOS2, respectively. The red line represents the MLS VMR. Error bars indicate 1  $\sigma$  standard deviation for each dataset. The number of coincident data are displayed at each point. (Middle) The absolute difference in the mean CH<sub>3</sub>CN VMR values between the SMILES AOS1/AOS2 and the MLS observations is calculated by Eq. 11. Blue broken lines indicate systematic errors theoretically derived in Sect. 3. (Right) The relative differences between CH<sub>3</sub>CN levels observed using SMILES and MLS methods is calculated by Eq. 12

study is the first of its kind to describe the data observed by the satellite instruments for the CH<sub>3</sub>CN VMR from the upper stratosphere to lower mesosphere with a much lower uncertainty of 20 ppt. Error analysis showed that random error was the dominant source of uncertainty (around 25 ppt at 15.7 hPa) in the measurement altitude range, resulting in a better precision by a factor of two or more than that of Aura/MLS. The uncertainty of air pressure broadening was the dominant systematic error source, with a maximum difference of 2.0 ppt (5%). The random error from single scan spectrum was more than two times larger than systematic error at 15.7 hPa, while the random error averaged with 100 spectra was comparable to systematic error. SMILES and Aura/MLS observations were in agreement in the stratosphere from 15.7 hPa to 4.8 hPa. At upper pressure levels, the difference between the two observations increased up to 35 ppt (260%) because of greater uncertainty of Aura/MLS observations, and because CH<sub>3</sub>CN levels were at their seasonal maximum. The theoretical systematic error and the relative difference of the SMILES measurements compared to MLS measurements were, respectively, 10 ppt and 35 ppt at altitudes



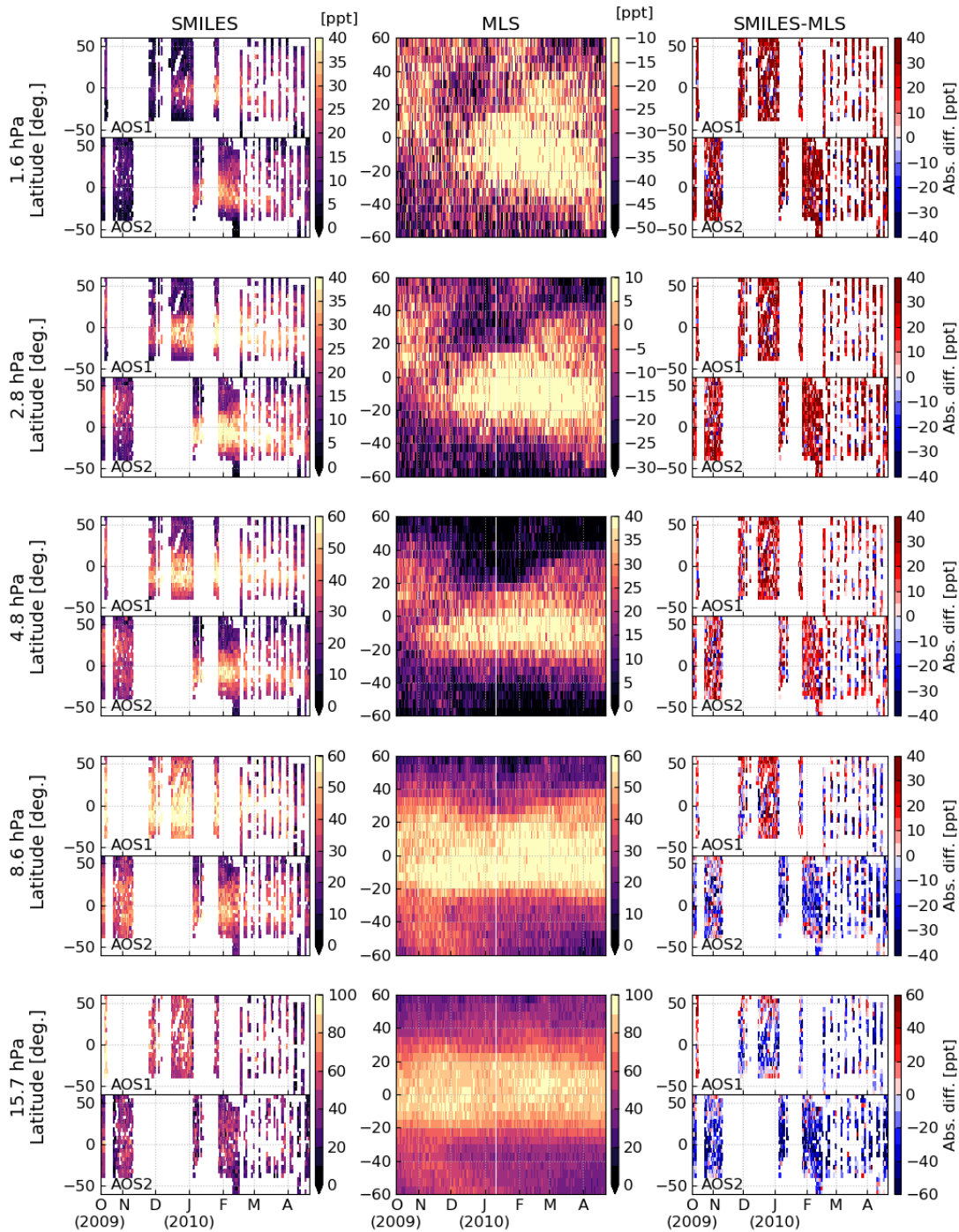


**Figure 10.** Seasonal variation of SMILES and MLS  $\text{CH}_3\text{CN}$  observations and the absolute difference for each pressure level, as a function of latitude. Observation date and latitude bins are 1 day and  $5^\circ$  grid

between 15.7 hPa and 1.6 hPa (28–44 km). Furthermore, the two AOSs show comparable errors ( $\sim 10$  ppt) at 0.93 hPa to 0.29 hPa (approximately 48–56 km) and at lower pressure levels, implying the reliability of SMILES  $\text{CH}_3\text{CN}$  observations.

*Data availability.* The SMILES data is available at <http://smiles.nict.go.jp/pub/data/index.html>. The MLS data is available at <https://mls.jpl.nasa.gov/data/>.

225 *Author contributions.* TF designed the study and performed the analysis. YK designed the study and provided the SMILES data. TOS provided the retrieval code and contributed to data analysis and interpretation. TY, SN, YU, and KT contributed to data analysis and reviewed the manuscript. NY supervised and reviewed the manuscript. TF wrote the manuscript with contributions from all coauthors.

*Competing interests.* The authors declare that there are no competing interests.

230 *Acknowledgements.* This work was conducted as a part of a research project titled 'R&D to Expand Radio Frequency Resources', which is supported by the Japanese Government through the Ministry of Internal Affairs and Communications (0155-0285, 0155-0093). We deeply appreciate Prof. Hideo Sagawa (Kyoto Sangyo University) for developing the SMILES L2r product v3.0.0. We are grateful to Atsushi Hirakawa and Kota Kuribayashi for supporting this study. We are grateful to Nathaniel Livesey for providing the MLS version 4.2.0 product.

## References

- Andreae, M. O.: Soot Carbon and Excess Fine Potassium: Long-Range Transport of Combustion-Derived Aerosols, *Science* (80-. ), 220,  
235 1148–1151, <https://doi.org/10.1126/science.220.4602.1148>, 1983.
- Arnold, F., Böhringer, H., and Henschen, G.: Composition measurements of stratospheric positive ions, *Geophys. Res. Lett.*, 5, 653–656,  
<https://doi.org/10.1029/GL005i008p00653>, 1978.
- Barath, F. T., Chavez, M. C., Cofield, R. E., Flower, D. A., Frerking, M. A., Gram, M. B., Harris, W. M., Holden, J. R., Jarnot, R. F.,  
Kloezeman, W. G., Klose, G. J., Lau, G. K., Loo, M. S., Maddison, B. J., Mattauch, R. J., McKinney, R. P., Peckham, G. E., Pickett,  
240 H. M., Siebes, G., Soltis, F. S., Suttie, R. A., Tarsala, J. A., Waters, J. W., and Wilson, W. J.: The Upper Atmosphere Research Satellite  
microwave limb sounder instrument, *J. Geophys. Res.*, 98, 10 751, <https://doi.org/10.1029/93JD00798>, 1993.
- Baron, P., Urban, J., Sagawa, H., Möller, J., Murtagh, D. P., Mendrok, J., Dupuy, E., Sato, T. O., Ochiai, S., Suzuki, K., Manabe, T., Nishibori,  
T., Kikuchi, K., Sato, R., Takayanagi, M., Murayama, Y., Shiotani, M., and Kasai, Y.: The level 2 research product algorithms for the Su-  
perconducting Submillimeter-Wave Limb-Emission Sounder (SMILES), *Atmos. Meas. Tech.*, 4, 2105–2124, <https://doi.org/10.5194/amt->  
245 4-2105-2011, 2011.
- Bernath, P.: Atmospheric Chemistry Experiment (ACE): An Overview, pp. 147–161, Springer Netherlands, <https://doi.org/10.1007/978-94->  
010-0832-7\_9, 2001.
- Crutzen, P. J. and Andreae, M. O.: Biomass Burning in the Tropics: Impact on Atmospheric Chemistry and Biogeochemical Cycles, *Science*  
(80-. ), 250, 1669–1678, <https://doi.org/10.1126/science.250.4988.1669>, 1990.
- 250 Crutzen, P. J., Heidt, L. E., Krasnec, J. P., Pollock, W. H., and Seiler, W.: Biomass burning as a source of atmospheric gases CO, H<sub>2</sub>, N<sub>2</sub>O,  
NO, CH<sub>3</sub>Cl and COS, *Nature*, 282, 253–256, <https://doi.org/10.1038/282253a0>, 1979.
- de Gouw, J. A.: Emission sources and ocean uptake of acetonitrile (CH<sub>3</sub> CN) in the atmosphere, *J. Geophys. Res.*, 108, 4329,  
<https://doi.org/10.1029/2002JD002897>, 2003.
- Eagan, R. C., Hobbs, P. V., and Radke, L. F.: Measurements of Cloud Condensation Nuclei and Cloud Droplet Size Distributions in the  
255 Vicinity of Forest Fires, *J. Appl. Meteorol.*, 13, 553–557, [https://doi.org/10.1175/1520-0450\(1974\)013<0553:MOCCNA>2.0.CO;2](https://doi.org/10.1175/1520-0450(1974)013<0553:MOCCNA>2.0.CO;2), 1974.
- Harrison, J. J. and Bernath, P. F.: ACE-FTS observations of acetonitrile in the lower stratosphere, *Atmos. Chem. Phys.*, 13, 7405–7413,  
<https://doi.org/10.5194/acp-13-7405-2013>, 2013.
- Kasai, Y., Sagawa, H., Kreyling, D., Dupuy, E., Baron, P., Mendrok, J., Suzuki, K., Sato, T. O., Nishibori, T., Mizobuchi, S., Kikuchi, K.,  
Manabe, T., Ozeki, H., Sugita, T., Fujiwara, M., Irimajiri, Y., Walker, K. A., Bernath, P. F., Boone, C., Stiller, G., Von Clarmann, T.,  
260 Orphal, J., Urban, J., Murtagh, D., Llewellyn, E. J., Degenstein, D., Bourassa, A. E., Lloyd, N. D., Froidevaux, L., Birk, M., Wagner, G.,  
Schreier, F., Xu, J., Vogt, P., Trautmann, T., and Yasui, M.: Validation of stratospheric and mesospheric ozone observed by SMILES from  
International Space Station, *Atmos. Meas. Tech.*, 6, 2311–2338, <https://doi.org/10.5194/amt-6-2311-2013>, 2013.
- Kikuchi, K. I., Nishibori, T., Ochiai, S., Ozeki, H., Irimajiri, Y., Kasai, Y., Koike, M., Manabe, T., Mizukoshi, K., Murayama, Y., Naga-  
hama, T., Sano, T., Sato, R., Seta, M., Takahashi, C., Takayanagi, M., Masuko, H., Inatani, J., Suzuki, M., and Shiotani, M.: Overview  
265 and early results of the Superconducting Submillimeter-Wave Limb-Emission Sounder (SMILES), *J. Geophys. Res. Atmos.*, 115, 1–12,  
<https://doi.org/10.1029/2010JD014379>, 2010.
- Knop, G. and Arnold, F.: Stratospheric trace gas detection using a new balloon-borne ACIMS method: Acetonitrile, acetone, and nitric acid,  
*Geophys. Res. Lett.*, 14, 1262–1265, <https://doi.org/10.1029/GL014i012p01262>, 1987.

- Li, Q., Jacob, D. J., Yantosca, R. M., Heald, C. L., Singh, H. B., Koike, M., Zhao, Y., Sachse, G. W., and Streets, D. G.: A global three-  
270 dimensional model analysis of the atmospheric budgets of HCN and CH<sub>3</sub>CN: Constraints from aircraft and ground measurements, *J. Geophys. Res.*, 108, 8827, <https://doi.org/10.1029/2002JD003075>, 2003.
- Livesey, N., Van Snyder, W., Read, W., and Wagner, P.: Retrieval algorithms for the EOS Microwave limb sounder (MLS), *IEEE Trans. Geosci. Remote Sens.*, 44, 1144–1155, <https://doi.org/10.1109/TGRS.2006.872327>, 2006.
- Livesey, N. J., Waters, J. W., Khosravi, R., Brasseur, G. P., Tyndall, G. S., and Read, W. G.: Stratospheric CH<sub>3</sub>CN from the UARS Microwave  
275 Limb Sounder, *Geophys. Res. Lett.*, 28, 779–782, <https://doi.org/10.1029/2000GL012144>, 2001.
- Livesey, N. J., Fromm, M. D., Waters, J. W., Manney, G. L., Santee, M. L., and Read, W. G.: Enhancements in lower stratospheric CH<sub>3</sub>CN observed by the Upper Atmosphere Research Satellite Microwave Limb Sounder following boreal forest fires, *J. Geophys. Res. Atmos.*, 109, n/a–n/a, <https://doi.org/10.1029/2003JD004055>, 2004.
- Marlon, J. R., Bartlein, P. J., Carcaillet, C., Gavin, D. G., Harrison, S. P., Higuera, P. E., Joos, F., Power, M. J., and Prentice, I. C.: Climate  
280 and human influences on global biomass burning over the past two millennia, *Nat. Geosci.*, 1, 697–702, <https://doi.org/10.1038/ngeo313>, 2008.
- Ochiai, S., Kikuchi, K., Nishibori, T., Manabe, T., Ozeki, H., Mizukoshi, K., Ohtsubo, F., Tsubosaka, K., Irimajiri, Y., Sato, R., and Shiotani, M.: Performance of JEM / SMILES in orbit, in: *Twenty-First Int. Symp. Sp. Terahertz Technol.*, pp. 179–184, 2011.
- Rienecker, M., Suarez, M., Todling, R., Bacmeister, J., Takacs, L., Liu, H.-C., Gu, W., Sienkiewicz, M., Koster, R., Gelaro, R., Stajner, I.,  
285 and Nielsen, J.: The GEOS-5 Data Assimilation System— Documentation of Versions 5.0.1, 5.1.0, and 5.2.0, Tech. Rep. December, 2008.
- Rodgers, C. D.: *Inverse Methods for Atmospheric Sounding: Theory and Practice*, World Scientific, London, vol. 2 edn., 2000.
- Sagawa, H., Sato, T. O., Baron, P., Dupuy, E., Livesey, N., Urban, J., Von Clarmann, T., De Lange, A., Wetzell, G., Connor, B. J., Kagawa, A., Murtagh, D., and Kasai, Y.: Comparison of SMILES ClO profiles with satellite, balloon-borne and ground-based measurements, *Atmos. Meas. Tech.*, 6, 3325–3347, <https://doi.org/10.5194/amt-6-3325-2013>, 2013.
- 290 Sato, T. O., Sagawa, H., Kreyling, D., Manabe, T., Ochiai, S., Kikuchi, K., Baron, P., Mendrok, J., Urban, J., Murtagh, D., Yasui, M., and Kasai, Y.: Strato-mesospheric ClO observations by SMILES: Error analysis and diurnal variation, *Atmos. Meas. Tech.*, 5, 2809–2825, <https://doi.org/10.5194/amt-5-2809-2012>, 2012.
- Sato, T. O., Sagawa, H., Yoshida, N., and Kasai, Y.: Vertical profile of  $\delta^{18}O$  from the middle stratosphere to lower mesosphere from SMILES spectra, *Atmos. Meas. Tech.*, 7, 941–958, <https://doi.org/10.5194/amt-7-941-2014>, 2014.
- 295 Schneider, J., Bürger, V., and Arnold, F.: Methyl cyanide and hydrogen cyanide measurements in the lower stratosphere: Implications for methyl cyanide sources and sinks, *J. Geophys. Res. Atmos.*, 102, 25 501–25 506, <https://doi.org/10.1029/97JD02364>, 1997.
- Seiler, W. and Crutzen, P. J.: Estimates of gross and net fluxes of carbon between the biosphere and the atmosphere from biomass burning, *Clim. Change*, 2, 207–247, <https://doi.org/10.1007/BF00137988>, 1980.
- Singh, H. B., Salas, L., Herlth, D., Kolyer, R., Czech, E., Viezee, W., Li, Q., Jacob, D. J., Blake, D., Sachse, G., Harward, C. N., Fuelberg, H.,  
300 Kiley, C. M., Zhao, Y., and Kondo, Y.: In situ measurements of HCN and CH<sub>3</sub>CN over the Pacific Ocean: Sources, sinks, and budgets, *J. Geophys. Res.*, 108, 8795, <https://doi.org/10.1029/2002JD003006>, 2003.
- Urban, J., Baron, P., Lautié, N., Schneider, N., Dassas, K., Ricaud, P., and De La Noë, J.: Moliere (v5): A versatile forward- and inversion model for the millimeter and sub-millimeter wavelength range, *J. Quant. Spectrosc. Radiat. Transf.*, 83, 529–554, [https://doi.org/10.1016/S0022-4073\(03\)00104-3](https://doi.org/10.1016/S0022-4073(03)00104-3), 2004.
- 305 Waters, J. W., Froidevaux, L., Harwood, R. S., Jarnot, R. F., Pickett, H. M., Read, W. G., Siegel, P. H., Cofield, R. E., Filipiak, M. J., Flower, D. A., Holden, J. R., Lau, G. K., Livesey, N. J., Manney, G. L., Pumphrey, H. C., Santee, M. L., Wu, D. L., Cuddy, D. T., Lay, R. R., Loo,

310 M. S., Perun, V. S., Schwartz, M. J., Stek, P. C., Thurstans, R. P., Boyles, M. A., Chandra, K. M., Chavez, M. C., Chen, G. S., Chudasama, B. V., Dodge, R., Fuller, R. A., Girard, M. A., Jiang, J. H., Jiang, Y., Knosp, B. W., Labelle, R. C., Lam, J. C., Lee, K. A., Miller, D., Oswald, J. E., Patel, N. C., Pukala, D. M., Quintero, O., Scaff, D. M., Van Snyder, W., Tope, M. C., Wagner, P. A., and Walch, M. J.: The Earth Observing System Microwave Limb Sounder (EOS MLS) on the aura satellite, *IEEE Trans. Geosci. Remote Sens.*, 44, 1075–1092, <https://doi.org/10.1109/TGRS.2006.873771>, 2006.